CrossMark

RESEARCH

Electrochemical degradation of C.I. Reactive Orange 107 using Gadolinium (Gd^{3+}), Neodymium (Nd^{3+}) and Samarium (Sm^{3+}) doped cerium oxide nanoparticles

K. Rajkumar[1,2] · M. Muthukumar[1] · R. V. Mangalaraja[3]

Abstract Ceria-based composites have been previously developed as functional electrolytes for high performance of solid oxide fuel cells that require high functional electrolyte materials that can provide high ion conductivity for sufficient current output. These composites display hybrid proton and oxygen ion conduction. We developed further composite electrolyte materials containing a catalyst such as rare earth elements; gadolinium (Gd^{3+}), neodymium (Nd^{3+}) and samarium (Sm^{3+}) doped ceria (Ce$_{0.8}$Gd$_{0.2}$O$_2$, Ce$_{0.8}$Nd$_{0.2}$O$_2$ and Ce$_{0.8}$Sm$_{0.2}$O$_2$) to investigate the electrochemical treatment of C.I. Reactive Orange 107. An experimental results showed that the nanomaterial plays an important role for the electrochemical oxidation of reactive dye, where Ce$_{0.8}$Gd$_{0.2}$O$_2$, Ce$_{0.8}$Nd$_{0.2}$O$_2$ and Ce$_{0.8}$Sm$_{0.2}$O$_2$ lead complete mineralization of selective dye. The results indicate that the overall performance in these schemes of operation is successful.

✉ K. Rajkumar
rajkumar_env@yahoo.co.in

1   Environmental Engineering and Technology Laboratory, Department of Environmental Sciences, Bharathiar University, Coimbatore 641 046, Tamilnadu, India

2   Chief Manager - Effluent Treatment Plant, M/s Senthil Papers and Boards Private Limited, Ikkaraithathappalli Village, Sathyamangalam, Erode 638 451, Tamilnadu, India

3   Department of Materials Engineering, Faculty of Engineering, University of Concepcion, Concepcion, Chile, Latin America

Introduction

The growth of industries and day-to-day changes in human activities have resulted in an increase in the volume and complexity of wastewater to the environment. The textile industry is one of the most polluting industries in terms of discharge volume and effluent composition [1]. Reactive dyes are extensively used in the textile industry due to the presence of reactive groups in their molecules which bind to fibers through covalent bonds. The main problem associated with the use of reactive dyes is their low affinity for fabrics resulting in relatively high dye concentrations in textile wastewater [2]. Reactive dyes exhibit a wide range of different chemical structures, primarily based on substituted aromatic and heterocyclic groups. Since reactive dyes are highly soluble in water, their removal from wastewater is difficult by conventional treatment processes [3–5].

In recent years, catalytic technologies have been described as an efficient means of eliminating organic pollutants. The technique generally uses a combination of oxidation (O$_3$, H$_2$O$_2$), irradiation, electron and catalyst as a means of generating hydroxyl radicals ($^{\cdot}$OH), superoxide radicals (O$_2^{-}$), hydroperoxyl (HO$_2^{\cdot}$) radicals, etc., at ambient temperature and pressure. The development of the electrocatalytic oxidation process is emerging as a strong alternative for conventional wastewater treatment. Recently, the importance of rare earth oxides as a catalyst is rapidly growing with new applications in different fields [6]. Since nanoparticles have uniform size and sharp size

🖉 Springer

distribution, they are easily prepared as a result of recent developments in nanoscience and nanotechnology. Cerium possesses good oxidizing behavior due to its high redox potential ($E^0 = 1.62$ V) [7]. Gadolinium (Gd^{3+}), neodymium (Nd^{3+}) and samarium (Sm^{3+}) are considered as the most effective dopants for ceria in terms of maximization of ionic conductivity [8].

Rare earth-doped cerium oxides have been shown to possess superior oxygen ionic conductivity in the range of intermediate to low temperatures [9]. Farmer et al. [10] proposed a kind of electro oxidation, mediated electro oxidation, in treating mixed and hazardous materials. In their works, metal ions, usually called mediators, are oxidized to an active, high valence state in the presence of an electric field, which in turn attack organic pollutants directly and may also produce hydroxyl free radicals that promote destruction of organic pollutants. The destruction of organics by the produced metal ion oxidant takes place through a number of intermediates and the reaction mechanism is moderately complex. As per the reported literature on electrocatalytic oxidation for the organic destruction reactions, free radicals such as ˙OH and ˙HO_2 are produced by the interaction between the oxidized metal ion and water, also called water oxidation reaction [10, 11].

In this study, an azo dye, C.I. Reactive Orange 107 (RO 107), was used as a model contaminant, for investigating the efficiency of electro oxidation and electrocatalytic oxidation using $Ce_{0.8}Gd_{0.2}O_2$, $Ce_{0.8}Nd_{0.2}O_2$ and $Ce_{0.8}Sm_{0.2}O_2$ composites as catalysts. The morphology of the catalyst was examined by using scanning electron microscope (SEM) and the evolution of nanocrystalline microstructure and grain size was analyzed using X-ray diffraction (XRD) and Raman spectroscopy. The characteristic absorption bands of RO 107 at 408 nm were investigated through the use of UV–visible spectroscopy, and mineralization was observed by total organic carbon (TOC) analysis. The functional groups were observed by FTIR and degradation by-products identified by the GC/MS techniques.

Materials and methods

Chemical reagents

Reactive dye (RO 107) was obtained from Jansons International Ltd., Mumbai, India. The properties and chemical structures of the dye are given in Table 1. In our earlier studies, we have already reported the combustion synthesis of Gd^{3+}, Nd^{3+} and Sm^{3+} doped cerium oxide nanocrystalline powders using citric acid as an organic fuel [12]. All chemicals were of analytical grade: hydrochloric acid,

sodium chloride, sodium hydroxide, dichloromethane, n-hexane (Loba chemie, Mumbai, India) and potassium bromide (Sigma-Aldrich) were used in this study. The graphite materials used were obtained from M/S Carbone Lorraine, Chennai, India. The electrical resistivity of graphite sheets was 0.001 Ω cm. The pH of the aqueous sample was measured using a pH meter (Susima pH meter AP-1 Plus, Chennai, India). All the solutions were prepared using deionized water.
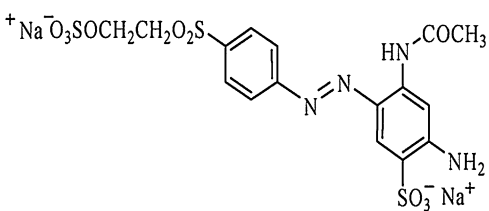
Experimental setup

The experiments were conducted on a batch process using a reactor having a capacity of 250 ml. Synthetic wastewater was prepared by dissolving RO 107 in double distilled water at a concentration of 500 μM. The experiments were carried out as per the optimum conditions obtained from our preliminary study (pH 9.4 and NaCl concentration 0.08) [13]. The schematic diagram of the complete system of electrochemical cell and electrode assembly is shown in Fig. 1. The graphite electrodes used as the anode and cathode were positioned vertically and parallel to each other with a space of 8 mm to reduce the ohmic losses. The graphite electrodes were 6.5×5.5 cm with contact surface area of 71.5 cm^2. The electric power was supplied with regulated DC power supply (Sri Sai Scientific, Coimbatore, India) and at a fixed current of 2.5A (current density of 34.96 mA cm^{-2}). For electrocatalytic oxidation process, 50 mg L^{-1} catalyst of Gd^{3+}, Nd^{3+} and Sm^{3+} doped cerium oxides ($Ce_{0.8}Gd_{0.2}O_2$, $Ce_{0.8}Nd_{0.2}O_2$ and $Ce_{0.8}Sm_{0.2}O_2$) respectively, was add to the suspension of the wastewater sample. The sample was constantly stirred using a magnetic stirrer (Superfit, Coimbatore, India).

Analytical techniques

The physical characterization of graphite electrode and catalyst was obtained from SEM [LaB6 JEM-2010 (HT)-FEF (HRTEM) England], XRD (X'Pert Pro, Philips X-ray diffracto meter) and Raman spectra (Horiba Jobin Raman spectrometer, Japan). The aqueous samples were taken before and after treatment for 10 and 20 min, time intervals and filtered using 0.45 μm cellulose acetate glass filter paper in the laboratory for the analysis of color using a UV–visible spectrophotometer (Shimadzu 3600, Japan) and total organic carbon content using a Shimadzu TOC analyzer (TOC-V$_{CPH}$ model, Japan). The functional groups were observed by FTIR (Nicolet 10, USA). The degradation by-products analysis using a GC system (HP model 5890 Series II, USA) was coupled with the MS system (HP model 5972 N, USA).

Table 1 Properties of the dye used for this study

C.I. name	Reactive Orange 107
Chemical structure	
Molecular formula	$C_{16}H_{16}N_4Na_2O_{10}S_3$
Molecular weight	566.49
λ max (nm) (water)	408
CAS No:	90597-79-8

Results and discussion

Electrode surface and catalyst structure characterization

A moderate difference was discussed in our preliminary study of the morphology of graphite anode electrode before and after the electrochemical process [14]. In the electrochemical oxidation process anode reaction, the substrate oxidation involves the transfer of one or more electrons from the substrate to the anode—direct electron transfer (DET). However, substrate oxidation rarely occurs without simultaneous oxidation of water, especially under amperostatic conditions. This opens up the possibility that attack on the substrate is initiated by reactive intermediates of water oxidation, such as hydroxyl radicals, hydrogen
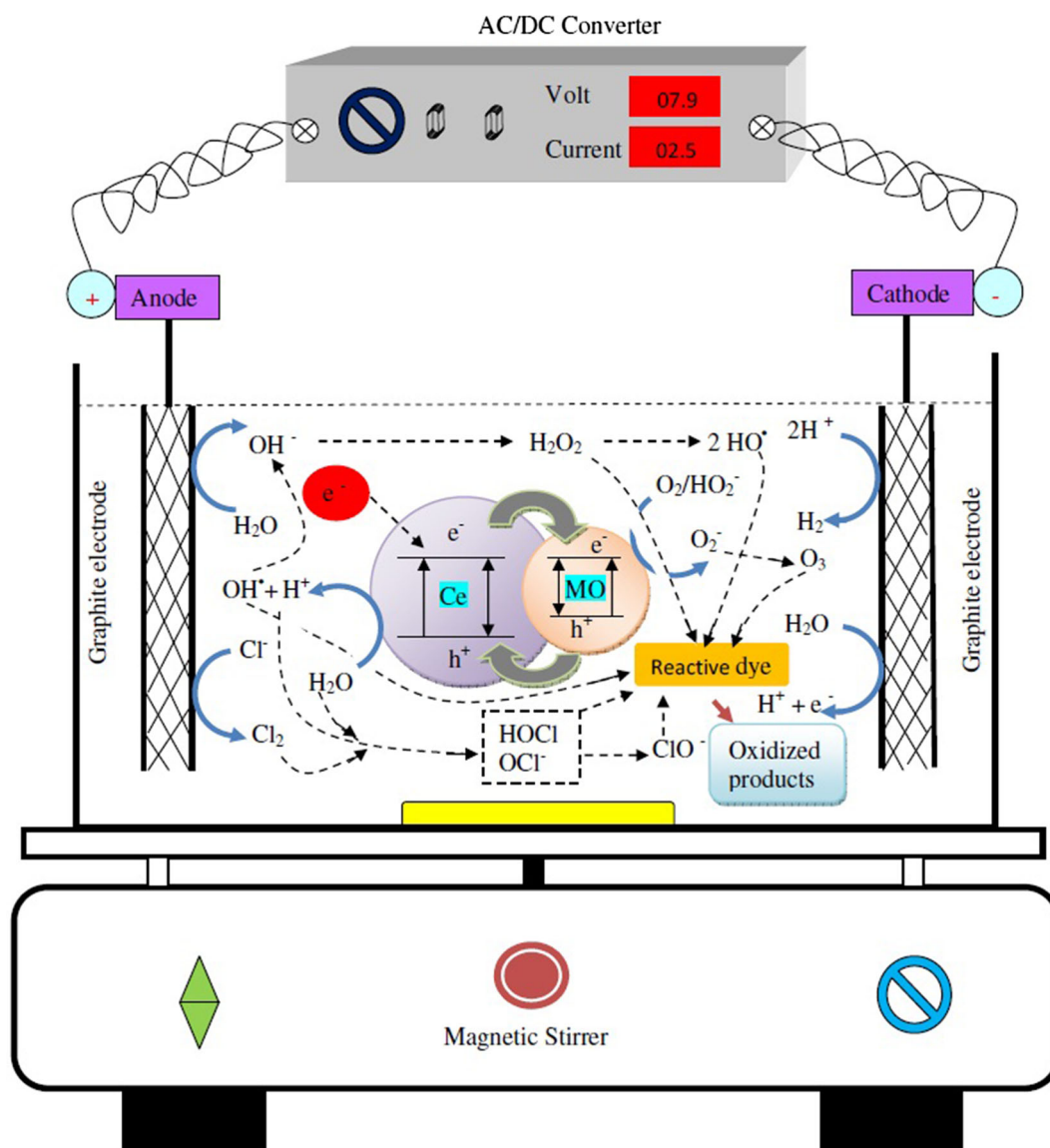

Fig. 1 Schematic representation of electrochemical oxidation processes for C.I. Reactive Orange 107 degradation

peroxide, hydroperoxy radicals and their basic conjugates, either free in solution or bound to the anode surface [15]. Figure 2 shows the images of Gd^{3+}, Nd^{3+} and Sm^{3+} doped cerium oxide and also morphologies such as sponge and flaky types. Microscopic observations confirmed that the powder also consists of porous agglomerates. The chemical analysis observed by the EDS attached to SEM for the calcined powders confirmed that the chemical composition was only $Ce_{0.8}Gd_{0.2}O_2$, $Ce_{0.8}Nd_{0.2}O_2$ and $Ce_{0.8}Sm_{0.2}O_2$, respectively.

XRD pattern studies

The crystalline nature and phase purity were examined using powder X-ray diffraction technique. The powder X-ray diffraction patterns of $Ce_{0.8}Gd_{0.2}O_2$, $Ce_{0.8}Nd_{0.2}O_2$ and $Ce_{0.8}Sm_{0.2}O_2$, respectively, of powders calcined at 700 °C are shown in Fig. 3. In the cases, the single-phase cubic structure of Gd^{3+}, Nd^{3+} and Sm^{3+} doped cerium oxide is noted (JCPDS No.: 34-394), and the structure was confirmed by the position of the different peaks at $2\theta = 27.8°$ (111), 33.9° (200), 48.3° (220), 57.4° (311), 59.7° (222), 70.0° (400), 77.4° (331) and 79.7° (420) lattice planes. Since there were no peaks representing free dopants, it can be confirmed that the Gd^{3+}, Nd^{3+} and Sm^{3+} dopant ions get substituted in the CeO_2 lattice [12]. The peaks were significantly broader due to small crystallite size. The average grain sizes were calculated from the XRD pattern according to Scherrer Eq. (1) [16]:

$$D = 0.94\lambda/(\beta^2 \text{sample} - \beta^2 \text{ref})^{1/2} \cos\theta, \qquad (1)$$

where D is the crystallite size diameter (nm), $\lambda = 1.54$Å, β is the full width at half maximum (FWHM) of a diffraction peak and β ref corresponds to the instrumental FWHM. The crystallite sizes were found to be 18.11, 14.04 and 18.24 nm, respectively. Generally, high surface area to volume ratio enhances the catalytic activity [17]. This can be explained in terms of an increase in the number of active sites per square meter [18], as well as yielding radicals on the catalyst surface.

Raman spectrum

The Raman spectrum of Gd^{3+}, Nd^{3+} and Sm^{3+} doped cerium oxide nanocrystals was analyzed by peaks resulting from scattering on optical phonon modes localized in the nanocrystal. The position and the width of the peaks strongly depend on the size and structure of the nanocrystal according to dispersion of localized modes. Figure 4 shows that cerium oxide had shifted its position at 461 cm^{-1}, slightly at 559 and 611 cm^{-1}; this shifting due to doping of Gd^{3+}, Nd^{3+} and Sm^{3+} was observed in the spectrum,

respectively. The same result was also reported by Taniguchi et al. [19]. So, Raman spectroscopy confirms the information on the presence of nano and micro clusters of crystal silicon in various surroundings and its size dispersion [20].

Comparative electro oxidation and electrocatalytic oxidation

UV–visible spectroscopy

A spectrophotometric scanning (200–700 nm) of RO 107 with a maximum absorbance peak at 408 nm was performed. Typical UV–visible spectra for untreated and treated aqueous solutions have been shown with changes in absorbance spectra in Fig. 5. The dye decolorization was apparent from a gradual decrease in absorbance at λ max. Absorbance spectral pattern and decrease rate were not similar to each other and to the initial one (0 min) for each applied catalyst, showing a change in the affinity of the dye for this nanocatalyst.

The results are shown in Fig. 5a. There were changes in the absorbance characteristics of RO 107 dye during the electrooxidation process, and the spectra showed a maximum absorbance at 408 nm in the visible region. The peak intensity decreases as the time increases during electrolysis. This may be because of the increasing duration of electrolysis, and the formation of secondary oxidant/reductant increases accordingly leading to the destruction of the chromophoric compounds. Figure 5 b shows the electrocatalytic oxidation of RO 107 in aqueous solution using Gd^{3+}, Nd^{3+} and Sm^{3+} doped cerium oxide nanoparticles. After 20 min of the oxidation process, there was a significant decrease in peak intensity almost equal to baseline showing complete decolorization. However, in both oxidation processes a small peak at 286 nm shows the formation of some phenolic derivative such as dye metabolites. Decrease in intensity of visible peak at λ max indicates disruption of the chromophoric group, i.e., azo group. However, the peaks between 220 to 260 nm at 20 min of electrolysis were the absorption of $\pi–\pi^*$ transitions due to amino group bonded to the naphthalene ring present in dye molecules [21, 22]. The appearance of a less intense peak at 286 nm refers to the formation of some phenyl derivative as metabolite, but it cannot be amino substituted as it is absorbed at the lower side of the UV spectra.

This may be due to direct or indirect oxidation through hydroxyl radicals generated by nanocatalysis (Fig. 1). A catalyst in an oxygen atom, eventually yielding more hydroxyl radicals, can enhance the decolorization of RO 107. This hypothesis was also reported by Matheswaran et al. [23]. For
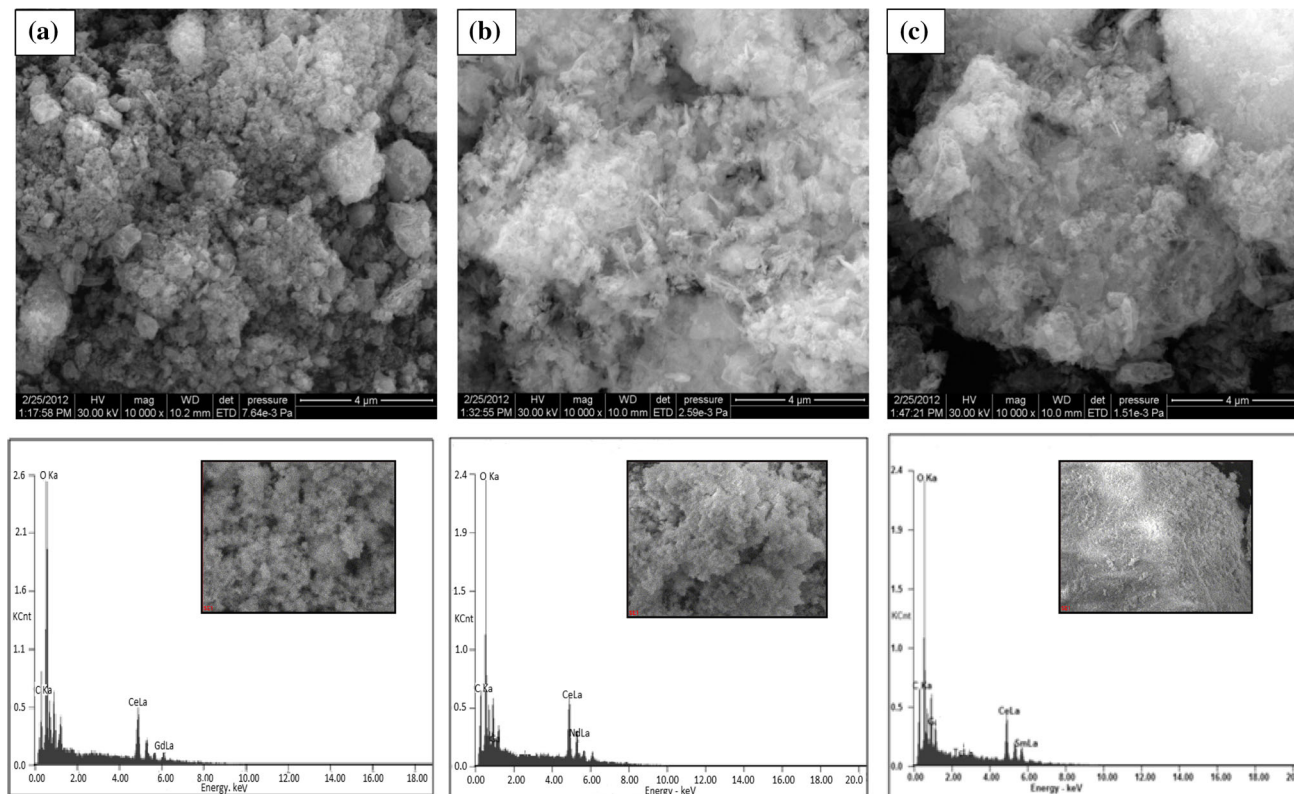
Fig. 2 SEM images of the surface attached chemical analysis spectrum of EDS for calcined **a** $Ce_{0.8}Gd_{0.2}O_2$, **b** $Ce_{0.8}Nd_{0.2}O_2$ and **c** $Ce_{0.8}Sm_{0.2}O_2$ powders prepared using citric acid
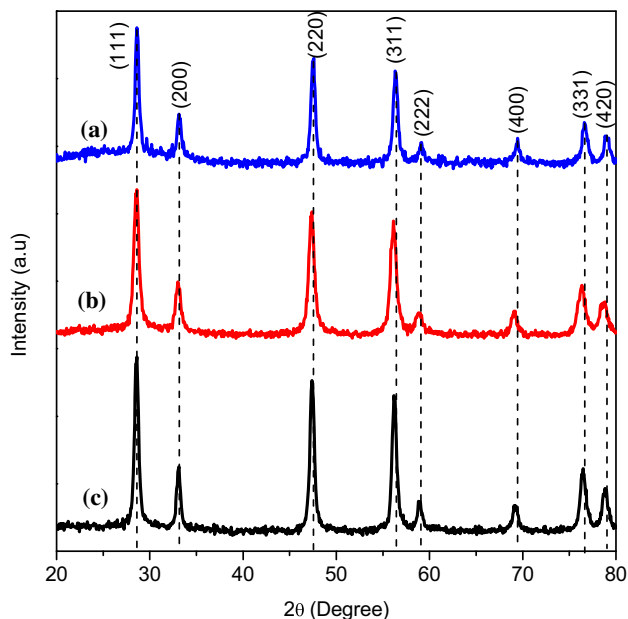

Fig. 3 X-ray diffraction patterns of calcined $Ce_{0.8}Gd_{0.2}O_2$, $Ce_{0.8}Nd_{0.2}O_2$ and $Ce_{0.8}Sm_{0.2}O_2$ (at 700 °C) powder

Fig. 4 Raman spectra of doped cerium oxide of Gd^{3+}, Nd^{3+} and Sm^{3+} after thermal annealing at 700 °C

both processes, the intensity of absorption at 625 nm declines extremely rapidly; however, the UV bands at 297 nm disappeared more slowly than the visible band. The disappearance
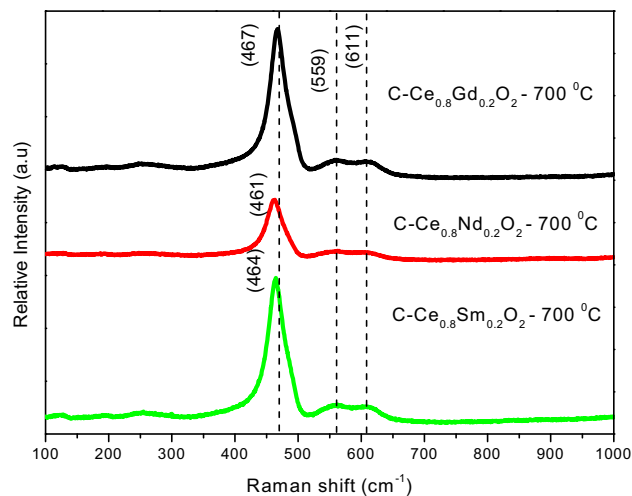
efficiency of the visible band is approximately double that of the UV band. The presence of reactive group showed that the C–Cl bond on the 1,3,5-triazine ring is the weakest bond, and the easy cleavage of this bond in the presence of catalyst indicates that the C–Cl bond on the ring is very susceptible to the hydroxyl radical attack. However, the peak was observed in UV region for the RO 107 under study confirm some
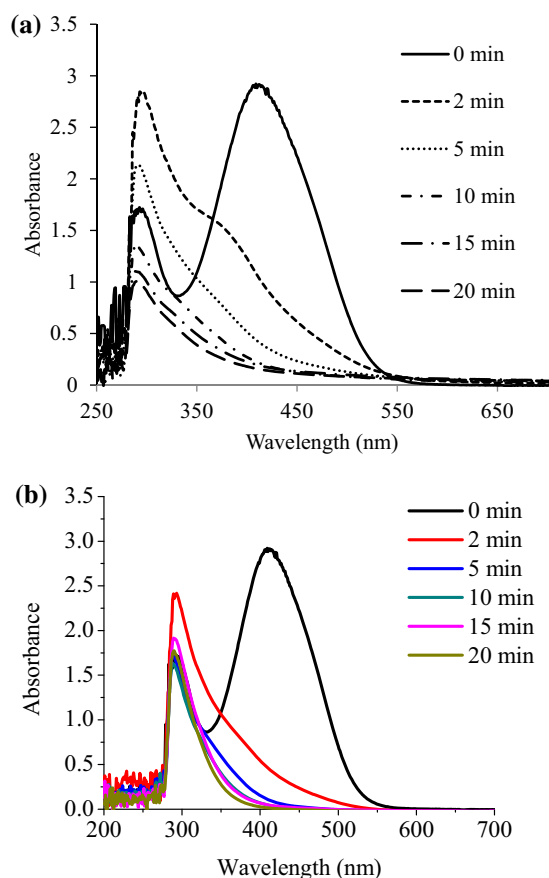
(a)

(b)

Fig. 5 UV-Vis spectra changes of RO 107 during electro oxidation (**a**) and electrocatalytic oxidation (**b**) at pH 9.4, NaCl concentration 0.08 and treatment time 20 min

metabolic by-products formed during electrocatalytic oxidation process. This represents the residual TOC present in the aqueous solution [24].

Mineralization studies

The comparative effects of electro oxidation and electrocatalytic oxidation on the changes of TOC in aqueous solutions of RO 107 dye are presented in Table 2. A concentration of RO 107 have 48.26 ppm in aqueous solutions by addition of Gd^{3+}, Nd^{3+} and Sm^{3+} doped cerium oxide catalyst under 20 min mineralization were achieved of 32.5 ppm (32.8 %), 31.0 ppm (35.7 %) and 32.4 ppm (32.9 %), respectively. During the electro oxidation process, TOC values were 24 % at 20 min. On comparing both the cases, TOC removal was 24 and 36 % for electro oxidation and electrocatalytic oxidation, respectively, at pH 9.4. In addition, the electrons may then react with species adsorbed on the surface, yielding radicals such as O_2^- as a result of the presence of hydroxyl groups, water and oxygen at the surface of the $Sm^{3+} > Gd^{3+} > Nd^{3+}$ doped cerium oxide particles.

Moreover, the color and TOC removal indicate that the electrogenerated active species are quite selective for the oxidation of the chromophore of the dye, and the oxidation of H_2O or OH^- to form O_2^- with high activity and indirectly degrade the dye molecules in aqueous solution. In the former, the catalyst couple merely plays the role of an electron carrier (mediator), whereas the transitory formation of catalyst–substrate adduct occurs in the latter [25]. In addition, the electrons may then react with species adsorbed on the surface, yielding radicals such as O_2^- as a result of the presence of hydroxyl groups, water, and oxygen at the surface of the Gd^{3+}, Nd^{3+} and Sm^{3+} doped cerium oxide particles (Fig. 1).

FTIR studies

To investigate the changes in the functional groups of the reactive dyes during the electro oxidation and electrocatalytic oxidation, Fig. 6 shows the IR spectra of the three reactive dyes before and after electrolysis at room temperature. The FTIR spectra of the dyes evidence absorption bands characteristic of the functional groups ($-NH_2$, $-OH$, $-SO_3Na$, $-COONa$, aromatic nuclei). The main absorption bands may be grouped as follows: the $-NH_2$ group evidences intense vibration bands in the 3300–3500 cm^{-1} region, and two intense deformation bands between 1590–1650 and 800–900 cm^{-1}, respectively; the phenolic group evidences the vibration of the O–H bond between 3200–3500 and 800–900 cm^{-1} (which overlaps with the ones of the $-NH_2$ group), and intense vibration bands, characteristic of the C–OH bond, between 1030–1085 and 1180–1260 cm^{-1}. The $-SO_3Na$ group evidences an intense band between 1120 and 1230 cm^{-1}, while the bands characteristic of the carboxylate group are present between 1700–1780 cm^{-1} (the C=O bond) and, respectively, 1050–1120 cm^{-1} (the C–O bond). The C–H bonds show bands between 2800 and 3100 cm^{-1}, while the main bands characteristic of the aromatic nuclei appear between 1400–1500 and 800–900 cm^{-1} [26].

In Fig. 6a, several bands can be distinguished in the spectra on initial RO 107 dyes. The peak at 3360 cm^{-1} account for O–H bond stretching assigned to H_2O that is always present and N–H group stretching that is assigned to the amine group of oleylamine. The appearance of a peak at 1513 cm^{-1} and 1457 cm^{-1} indicates the presence of the azo group, and the secondary and primary amines, respectively. Other peaks were also observed at 1250–1000 cm^{-1} (S–O stretching and aromatic C–H bending). The peaks at 617, 634, 751 and 550.8 cm^{-1} account for aromatic or benzene ring. Figure 6b shows the IR spectra after treatment. The peaks are at 2360 and 2341 cm^{-1} for O=C=O and 1384 cm^{-1} for SO_2 stretching. The peaks at 1514.3, 1457.3, 1232.2 and 1136.1 cm^{-1}

Table 2 An effect of oxidation by electro oxidation and electrocatalytic oxidation on changes of total organic carbon in aqueous C.I. Reactive Orange 107 dye solution

Name of dye	Before oxidation	ηTOC (%)							
	TOC (ppm)	Electro oxidation		Electrocatalytic oxidation					
	0 min	10 min	20 min	10 min			20 min		
				Gd^{3+}	Nd^{3+}	Sm^{3+}	Gd^{3+}	Nd^{3+}	Sm^{3+}
Reactive Orange 107	48.26	19.35	24.03	30.0	24.8	28.6	32.8	35.7	32.9

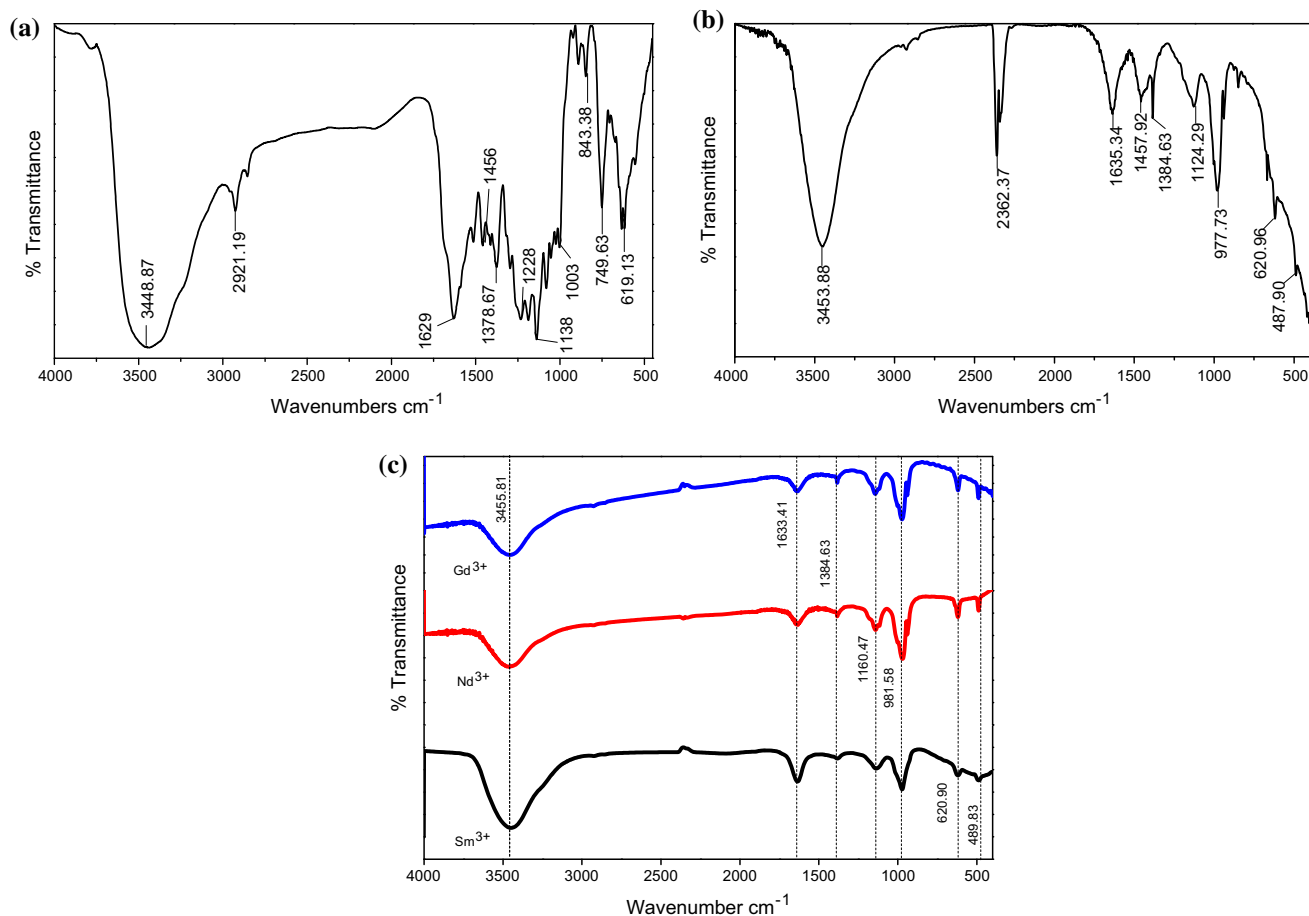η the reduction of TOC values (%)

Fig. 6 FTIR spectrum of the C.I. Reactive Orange 107 powder (**a**), after electro oxidation (**b**) and electrocatalytic oxidation (**c**) with 50 mg L^{-1} of catalyst at pH 9.4, NaCl concentration 0.08 M and 20 min

completely disappear and peaks at 939 and 811 cm^{-1} account for $ClO_3{}^{-}$ and OCl^{-}, which may generally be present in the hypochlorite solution. The formation of peaks at 1632.7 cm^{-1} and 980.5 cm^{-1} indicate the aliphatic secondary amine, C–O–H stretching and ·OH.

An electrocatalytic oxidation process of RO 107 with Gd^{3+}, Nd^{3+} and Sm^{3+} doped cerium oxide, after electrolysis is shown in Fig. 6c. The formation of peaks at 1648 cm^{-1} was observed, which can be assigned as the

stretching of C=O in carboxylic groups, aldehydes or ketones [27–29]. Furthermore, a new absorption peak of 977.7 and 619.1 cm^{-1} indicates the aliphatic secondary amine, C–O–H stretching and ·OH. This suggested the cleavage of the vinylsulfonyl group ($-SO_2CH_2CH_2OSO_3{-}$Na) after electrocatalytic oxidation.

This variation in the FTIR spectra can be explained by the complete degradation of organic compound and formation of other intermediate organic compounds.

GC–MS studies

Quantitative analysis of the intermediates is helpful to get a better understanding of the mechanism of the electro oxidation and electrocatalytic oxidation process. The intermediate compounds formed during the degradation of RO 107 were identified by GC–MS. The more frequently identified compounds during the electrolysis are shown in Table 3. Figure 7 also shows that, after 20 min of the oxidation process, the major fragments were generated in both degradation processes. Figure 7a shows that the electrooxidation decomposition of RO 107 was firstly initiated by the cleavage of –N=N–, with the hydrazo derivative, namely S1 and S2, as possible intermediates. The sulfonic group in the S1 molecule renders it thermally stable and highly soluble in water. Afterward, the sulfonic group underwent further desulfonation, resulting in the formation of benzoquinone and phenol that was further oxidized to organic acids and then completely mineralized as many pointed out by literature [30–32].

In the case of electrocatalytic oxidation, two different pathways such as S1 and S2 (Fig. 7b) were proposed for the degradation of RO 107. The degradation of the dye under catalytic conditions causes significant mineralization which results in the formation of substituted N-(3-Aminophenyl)-acetamide, benzene-1,3-diamine, benzene-1,3-diamine, benzenediazonium, benzene, phenol and other lower molecular weight compounds. The chromophore in the dye molecule should be split in the first step. The bonds C–N and C–N in the RO 107 molecule were probably cleaved by free radical attack, which led to the decoloring of RO 107 in the bulk solution.

However, the results indicated that the azo group might be converted to ammonia and nitrate ions simultaneously. Takahashi et al. [33] confirmed that only trace amounts of nitrate and ammonium ions can be determined. Phenols are highly reactive substrates in aromatic electrophilic substitution, since the non-bonded electrons of the hydroxyl group stabilize the sigma complex that is formed due to an electrophilic attack in the ortho or para position. A substitute electron donor as –OH in the phenol molecule activates mainly the ortho and para positions, and a substitute electron subtracts or the group –COOH disables these positions. Phenols oxidize producing aromatic ketones or diketones named quinones; once the quinone is formed, the ring opening takes place to produce carboxylic acids. Tauber et al. [34] reported that the degradation of azo dyes using fungus and ultrasound will lead to the formation of the reduction products such as phenol, CO_2 and carboxylic acids such as oxalic, malonic, formic, propionic and acetic acid and, moreover, the degradation of phenol produces catechol, hydroquinone and benzoquinone.

These compounds later underwent deep degradation to form benzene-type intermediates, the further oxidation of which resulted in aromatic ring cleavage and generation of aliphatic acids, such as hexanoic acid, enanthic acid and hexylacetic acid. Finally, these organic acids were decomposed to CO_2 to accomplish the entire mineralization process. The mechanism of the electrocatalytic oxidation process using Gd^{3+}, Nd^{3+} and Sm^{3+} doped cerium oxides is briefly explained as follows.

The electrogenerated electrons can directly reduce the dye or react with electron acceptors such as O_2 adsorbed on the catalyst surface or dissolved in water to superoxide radical anion ($O_2^{\cdot-}$). Besides, the electrogenerated holes can oxidize the organic molecule to form R^+ or react with OH^- and H_2O oxidizing them into $^{\cdot}OH$. Other highly oxidant species such as peroxide radicals are reported also to be responsible for the heterogeneity. The relevant reactions at the semiconductor surface causing the degradation of dyes can be summarized as follows:
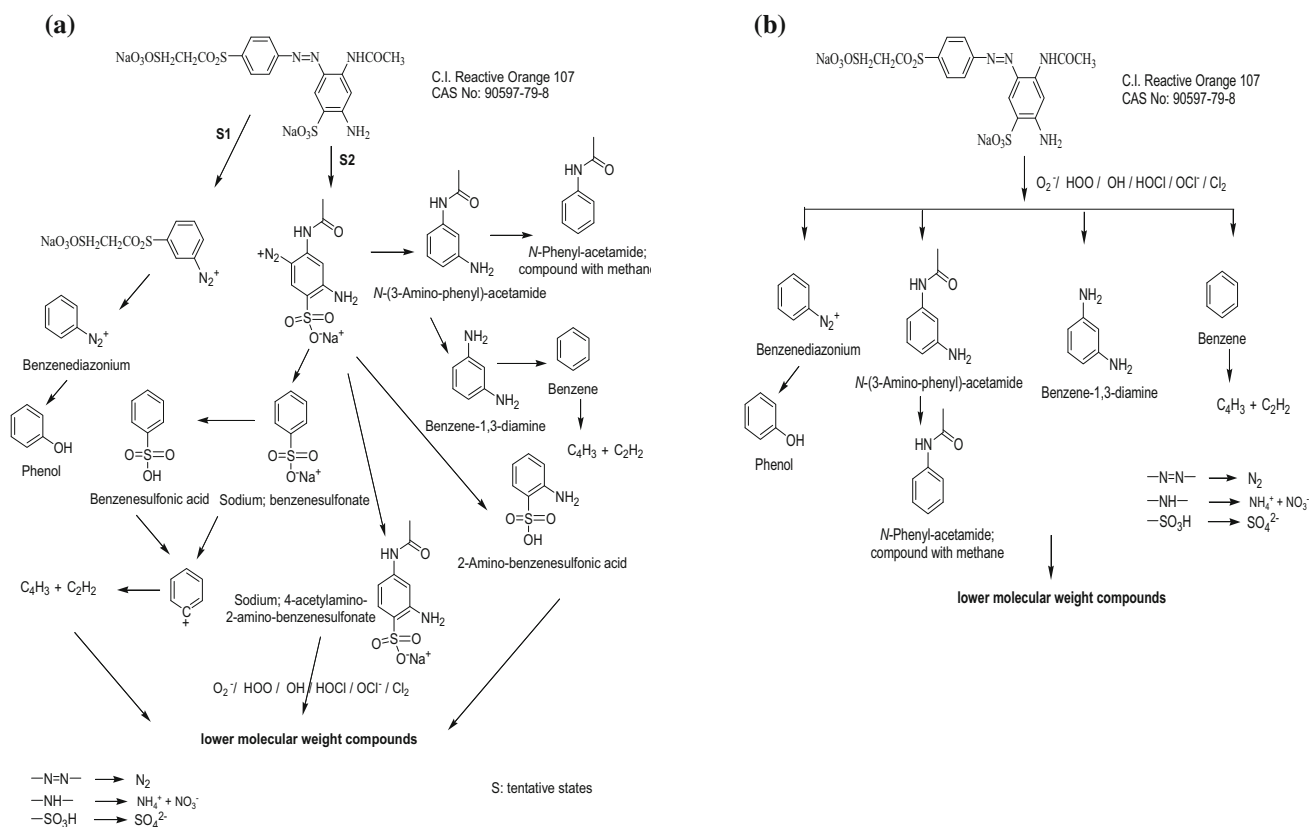
$$\text{Dye} + ^{\cdot}\text{OH}, O_2^{\cdot-} \text{ or } HO_2^{\cdot} \rightarrow SO_4^{2-}, NO_3^-, NH_4^+, CO_2 \text{ and } H_2O.$$
(2)
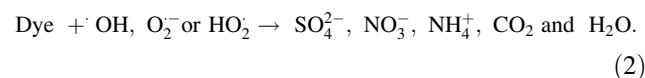
These radicals ($^{\cdot}OH$, $O_2^{\cdot-}$ and $HO_2^{\cdot}$) are very strong oxidizing agents and they are able to decompose the dyes to the oxidation products. Eventually, the parent compounds and their intermediates will be oxidized into inorganic products (SO_4^{2-}, NO_3^-, NH_4^+), CO_2 and water [35–38]. Even if this mechanism was involved as a primary step in the degradation of dyes under study, amines formed as a result were further oxidized leading to low molecular weight non-toxic simpler organic compounds. In this study, it could be supposed that if azo oxidation acts as first part and aniline-like amino derivatives are formed on one side and naphthalene derivatives on the other side with further degradation, particularly in C–N bond, it would be broken and domination would result in the form of oxidized phenyl derivatives or naphthyl derivatives. Phenolics like catechols and resorcinols, easily mineralized to aliphatic and aromatic carboxylic acid through ring opening. These carboxylic acids can easily be changed to CO_2 and H_2O leading to complete mineralization of recalcitrant organic dye molecules [39, 40].

Overall, the electrolytic decomposition of C.I RO 107 in the electrocatalytic system can be described by a series of consecutive degradation steps. The TOC measurements have shown during this study that the reaction follows an evolution by way of a total mineralization. It is also to be mentioned that the final degradation products were mineral ions such as NH_4^+, NO_3^- and SO_4^{2-} according to the substituent groups included in the initial molecule, as well as CO_2 and H_2O.

Table 3 List of intermediate compounds generated during electro oxidation and electrocatalytic oxidation of C.I. Reactive Orange 107 dye solution

S. no	Reactive Orange 107		EO	ECO		
	Compound	Molecular weight	Without catalyst	Gd^{3+}	Nd^{3+}	Sm^{3+}
1	Sodium, 4-acetylamino-2-amino-benzenesulfonate	253	√	–	–	–
2	2-Amino-benzenesulfonic acid	195	√	–	–	–
3	Sodium, benzenesulfonate	158	√	–	–	–
4	Benzenesulfonic acid	158	√	–	–	–
5	N-(3-Amino-phenyl)-acetamide	151	√	√	√	√
6	2-Amino-benzenesulfonic acid	195	√	–	–	–
7	N-Phenyl-acetamide, compound with methane	135	√	–	√	–
8	Benzene-1,3-diamine	108	√	√	√	√
9	Benzenediazonium	105	√	√	–	√
10	Phenol	94	√	–	–	√
11	Benzene	78	√	√	–	√
12	Acetylene	26	–	–	√	√

Fig. 7 The probable degradation pathway of C.I. Reactive Orange 107 during (**a**) electro oxidation and (**b**) electrocatalytic oxidation

Conclusions

The rare earth (Gd^{3+}, Nd^{3+} and Sm^{3+}) doped cerium oxide has been successfully applied in textile dye decolorization and degradation of azo dye RO 107, which showed a significant effect on the electrocatalytic activity. The degradation of high-concentration and high-chromoselective dye solution is realized through the electro oxidation and electrocatalytic oxidation processes. UV-Vis and FTIR spectral studies confirmed that the proposed

electrochemical degradation process is an effective method for the decolorization and degradation. Mineralization studies of RO 107 shows the increase in TOC removal values from 32 to 35.7 % after 20 min of electrocatalytic oxidation using Gd^{3+}, Nd^{3+} and Sm^{3+} doped ceria oxides, and the intermediates detected by GC–MS, the azo bond of the dye structure was the first potentially broken when the azo bond was attacked, which led to the decolorization of the dye. With the help of hydroxyl radical and other radicals, the intermediates continued to be degraded to carbon dioxide and water, which led to the mineralization of the dye solution. Combining cerium-doped Gd^{3+}, Nd^{3+} and Sm^{3+} oxides with electro oxidation is effective for the removal of pollutants from textile dye wastewater in short duration. This technique can be explored further for alternate strategies of wastewater treatment.

The results indicate that $Ce_{0.8}Gd_{0.2}O_2$, $Ce_{0.8}Nd_{0.2}O_2$ and $Ce_{0.8}Sm_{0.2}O_2$ act as a co-catalyst for electrocatalytic oxidation processes. The main electrochemical reaction for the enhanced rate is the rapid inhibition of the electrocharge carriers by catalyst. The beneficial effect of electron acceptor is to generate more number of radicals, which in turn degrade the pollutants effectively through the radical chain branching mechanism. Further work was needed to test on industrial scale and other organic wastewater.

References

1. Mohan N, Balasubramanian N (2006) In situ electrocatalytic oxidation of acid violet 12 dye effluent. J Hazard Mater 136:239–243
2. Siddique M, Farooq R, Khan ZM, Khan Z, Shaukat SF (2011) Enhanced decomposition of reactive blue 19 dye in ultrasound assisted electrochemical reactor. Ultra Sonochem 18:190–196
3. Gouvea CA, Wypych F, Moraes SG, Duran N, Nagata N, Peralta-Zamora P (2000) Semiconductor-assisted photocatalytic degradation of reactive dyes in aqueous solution. Chemosphere 40(4):433–440
4. Tang C, Chen V (2004) The photocatalytic degradation of reactive black 5 using TiO2/UV in an annular photoreactor. Water Res 38(11):2775–2781
5. Lucas M, Mertens V, Corbisier A, Vanhulle S (2008) Synthetic dyes decolourisation by white rot fungi: development of original microtitre plate method and screening. Enzym Microb Technol 42:97–106
6. Trovarelli A, de Leitenburg C, Boaro M, Dolcetti G (1999) The utilization of ceria in industrial catalysis. Catal Today 50:353–367
7. Nelson N, Neustedter T, Oberg S, Varela J (2000) The cerox process: new technology for organic hazardous waste destruction. In: Proceedings of the Symposium on Emerging Technologies: Waste Management in the 21st Century, American Chemical Society Meeting, San Francisco
8. Molenda J (2006) Lithium-ion batteries—state of art novel phospho-olivine cathode materials. Mater Sci Pol 24(1):61–67
9. Liu QL, Chan SH, Fu CJ, Pasciak G (2009) Fabrication and characterization of large –size electrolyte/anode bilayer structures for low-temperature solid oxide fuel cell stack dased on gadolinium doped ceria electrolyte. Electrochem Commun 11:871–874
10. Farmer JC, Wang FT, Hawley-Fedder RA, Lewis PR, Summers LJ, Foiles L (1992) Electrochemical treatment of mixed and hazardous wastes: oxidation of ethylene glycol and benzene by silver(II). J Electrochem Soc 139:654–662
11. Steele DF (1990) Electrochemical destruction of toxic organic industrial waste. Platin Met Rev 34:10–14
12. Manglaraja RV, Ananthakumar S, Uma K, Jimenez RM, Lopez M, Carlos CP (2009) Microhardness and fracture toughness of $Ce_{0.9}Gd_{0.1}O_{1.95}$ for manufacturing solid oxide electrolytes. Mater Sci Eng A 517:91–96
13. Rajkumar K, Muthukumar M (2012) Optimization of electro-oxidation process for the treatment of Reactive Orange 107 using response surface methodology. Environ Sci Pollut Res 19:148–160
14. Rajkumar K, Muthukumar M (2015) Response surface optimization of electro-oxidation process for the treatment of C.I. Reactive Yellow 186 dye: reaction pathways. Appl Water. doi:10.1007/s13201-015-0276-0
15. Rueffer M, Bejan D, Bunce NJ (2011) Graphite: an active or an inactive anode. Electrochim Acta 56:2246–2253
16. Cullity BD (1978) Elements of X-ray diffraction, 2nd edn. Addison-Wesley, Boston
17. Hoffmann AJ, Mills G, Yee H, Hoffmann MR (1992) Q-sized CdS: synthesis, characterisation, and efficiency of photoinitiation of polymerisation of several vinylic monomers. J Phys Chem 96:5546–5552
18. Xu N, Shi Z, Fan Y, Dong J, Shi J, Hu MZ-C (1999) Effect of particle size of TiO2 on photocatalytic degradation of methylene blue in aqueous suspension. Ind Eng Chem Res 38:373
19. Taniguchi T, Watanabe T, Sakamoto N, Matsushita N, Yoshimura M (2008) Aqueous route to size-controlled and doped organophilic ceria nanocrystals. Cryst Growth Des 8(10):3725–3730
20. Volodin VA, Efremov MD, Gritsenko VA, Kochubei SA (1998) Raman study of silicon nanocrystals formed in SiNx films by excimer laser or thermal annealing. Appl Phys Lett 73:1212
21. Pajootan E, Arami M, Rahimdokht M (2014) Discoloration of wastewater in a continuous electro-Fenton process using modified graphite electrode with multi-walled carbon nanotubes/surfactant. Sep Purif Technol 130:34–44
22. Xiong Y, Strunk PJ, Xia HY, Zhu XH, Karlsson HT (2001) Treatment of dye wastewater containing acid orange II using a cell with three-phase three dimensional electrode. Water Res 35:4226–4230
23. Matheswaran M, Balaji S, Chung SJ, Moon IS (2007) Mineralization of phenol by Ce(IV)-mediated electrochemical oxidation in methanesulphonic acid medium: a preliminary study. Chemosphere 69:325–331

24. Oliveiraa GR, Fernandesa NS, Meloa JV, Silva DR, Urgegheb C, Martinez-Huitlea CA (2011) Electrocatalytic properties of Ti-supported Pt for decolorizing and removing dye from synthetic textile wastewaters. Chem Eng J 168:208–214

25. Cheung KC, Wong WL, Ma DL, Lai TS, Wong KY (2007) Transition metal complexes as electrocatalysts—development and applications in electro-oxidation reactions. Coord Chem Rev 251:2367–2385

26. Ayram M, Mateescu GD (1978) Infrared spectroscopy: applications in organic chemistry. Krieger Publishing, Huntington

27. Bauer C, Jacques P, Kalt A (2001) Photooxidation of an azo dye induced by visible light incident on the surface of TiO_2. J Photochem Photobiol A Chem 140:87–92

28. Zhang SJ, Yu HQ, Li QR (2005) Radiolytic degradation of Acid Orange 7: a mechanistic study. Chemosphere 61:1003–1011

29. Li GT, Qu JH, Zhang XW, Liu HJ, Liu HN (2006) Electro-chemically assisted photocatalytic degradation of Orange II: influence of initial pH values. J Mol Catal A Chem 259:238–244

30. Liu L, Zhao GH, Wu MF, Lei YZ, Geng R (2009) Electro-chemical degradation of chlorobenzene on boron-doped diamond and platinum electrodes. J Hazard Mater 168:179–186

31. Huang WJ, Li ZW, Lin YJ, Yang CH, Liou YJ (2012) Electro-catalytic characterization and dye degradation of $Ti_{1−x}(Bi)xO_2$ in acidic solution. Cerami Int 36(6):4631–4634

32. Sahinkaya S (2013) COD and color removal from synthetic textile wastewater by ultrasound assisted electro-Fenton oxidation process. J Ind Eng Chem 19(2):601–605

33. Takahashi N, Nakai T, Satoh Y, Katoh Y (1994) Variation of biodegradability of nitrogenous of organic compounds by ozonation. Water Res 28:1563–1570

34. Tauber MM, Guebitz GM, Rehorek A (2005) Degradation of azo dyes by laccase and ultrasound treatment. Appl Environ Microbiol 71:2600–2607

35. Xu X, Liao P, Yuan S, Tong M, Luo M, Xie W (2013) Cu-catalytic generation of reactive oxidizing species from H_2 and O_2 produced by water electrolysis for electro-fenton degradation of organic contaminants. Chem Eng J 233:117–123

36. Tanaka K, Padermpole K, Hisanaga T (2000) Photocatalytic degradation of commercial azo dyes. Water Res 34(1):327–333

37. Galindo C, Jacques P, Kalt A (2000) Photodegradation of the aminoazobenzene acid orange 52 by three advanced oxidation processes: UV/H_2O_2, UV/TiO_2 and VIS/TiO_2 comparative mechanistic and kinetic investigations. J Photochem Photobiol A Chem 130:35–47

38. Daneshvar N, Salari D, Khataee AR (2003) Photocatalytic degradation of azo dye acid red 14 in water:investigation of the effect of operational parameter. J Photochem Photobiol A Chem 157:111–116

39. Soni BD, Ruparelia JP (2013) Decolourization and mineralization of Reactive black-5 with transition metal oxide coated electrodes by electrochemical oxidation. Procedia Eng 51:335–341

40. Ghenymy AE, Centellas F, Garrido JA, Rodriguez RM, Sires I, Cabot PL, Brillas E (2014) Decolorization and mineralization of Orange G azo dye solutions by anodic oxidation with a boron-doped diamond anode in divided and undivided tank reactors. Electrochim Acta 130:568–576